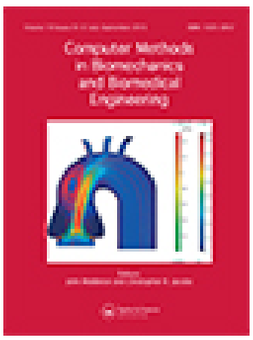

Taylor & Francis
Taylor & Francis Group

Computer Methods in Biomechanics and Biomedical Engineering

ISSN: 1025-5842 (Print) 1476-8259 (Online) Journal homepage: https://www.tandfonline.com/loi/gcmb20

Improved accuracy in 3D analysis using DLT after lens distortion correction

Marcel M. Rossi, Amanda P. Silvatti, Fabio A.S. Dias & Ricardo M.L. Barros

To cite this article: Marcel M. Rossi, Amanda P. Silvatti, Fabio A.S. Dias & Ricardo M.L. Barros (2015) Improved accuracy in 3D analysis using DLT after lens distortion correction, Computer Methods in Biomechanics and Biomedical Engineering, 18:9, 993-1002, DOI: 10.1080/10255842.2013.866231

To link to this article: https://doi.org/10.1080/10255842.2013.866231

Computer Methods in Biomechanics and Biomedical Engineering, 2015
Vol. 18, No. 9, 993–1002, http://dx.doi.org/10.1080/10255842.2013.866231

Taylor & Francis
Taylor & Francis Group

Improved accuracy in 3D analysis using DLT after lens distortion correction

Marcel M. Rossi[a]*, Amanda P. Silvatti[b1], Fabio A.S. Dias[c2] and Ricardo M.L. Barros[b3]

[a]*School of Sport Science, Exercise and Health, The University of Western Australia, 35 Stirling Highway, Crawley, Perth 6009, Australia;* [b]*Faculty of Physical Education, University of Campinas, Avenida Érico Veríssimo, 701, Cidade Universitária Zeferino Vaz, Barão Geraldo, Caixa Postal (P.O. BOX) 6134 Cep 13083-851, Campinas, SP, Brazil;* [c]*Laboratoire d'Informatique Gaspard-Monge, ESIEE, Paris, France*

(*Received 18 April 2012; accepted 12 November 2013*)

This study aimed at assessing the applicability of a robust method to determine and correct lens distortion before using the direct linear transformation (DLT) algorithm in three-dimensional motion analysis. The known length of a rigid bar was reconstructed under different conditions of working volume (interpolation or extrapolation), number of cameras (2 or 4), position of the cameras (wide or narrow angle between optical axes), camera focal distance (4 or 8 mm) and number of control points (CPs; 8, 12, 18 or 162), through four different camera set-ups. The accuracy (percent root mean square error) of Set-up 2 (non-extrapolated working volume; two cameras; 4 mm focal distance; narrow optical axes angle) decreased with less CPs (162: 0.73%; 8: 2.78%). Set-up 1 (non-extrapolated working volume; two cameras; 8 mm focal distance; wide optical axes angle), Set-up 3 (Set-ups 1 and 2 used simultaneously) and Set-up 4 (extrapolated working volume; two cameras; 4 mm focal distance; wide optical axes angle) showed minor differences in accuracy across groups of CPs, with maximum values of 0.84%, 1.20% and 1.71%, respectively. Random errors were the main source of decreased accuracy of Set-ups 2 and 4.The proposed procedure enables accurate results with no modification in the DLT-based analysis system, even with smaller calibration frames, less CPs and wide field-of-view cameras.

Keywords: DLT; lens distortion; extrapolation; focal distance; control points

Introduction

Image-based analysis systems have been widely used in sports biomechanics. Even with the recent advent of more modern passive optical analysis systems such as Vicon™ and Elite™, image-based systems may yet be regarded as a more feasible option for in-field analyses, given the limitations of using red and infrared cameras outdoor (Elliott and Alderson 2007). The direct linear transformation (DLT) proposed by Abdel-Aziz and Karara (1971) is probably the most widely used and discussed technique for three-dimensional (3D) reconstruction of human movements through image-based analyses (Allard et al. 1995). Examples can be found in several sport activities, such as tennis (Elliott et al. 2003; Fleisig et al. 2003), golf (Coleman and Rankin 2005) and swimming (Arellano et al. 1994; Sanders et al. 1995; Lauder et al. 2001; Gourgoulis, Aggeloussis, Vezos, et al. 2008).

As in any other measurement technique, the DLT is susceptible to systematic and random errors. One important source of systematic errors is the lens distortion, which deforms the image as a result of the deviation that the light ray suffers whenever it passes from the air to the lens and then from the lens back to the air. The DLT algorithm is based on the pin hole camera model, assuming that the collinearity condition (i.e. a point in the real object is projected by a straight line passing through the projection centre onto the sensor of the camera) is not violated (Heikkila and Silven 1997), whereas the relationship between the real and the distorted image is nonlinear (Brown 1971); therefore, the DLT cannot correct the errors caused by lens distortion, it just provides the best-fit solution for a given set-up (Kwon and Casebolt 2006). A series of procedures are adopted to ensure those errors are minimised, like using as many control points (CPs) as possible to surround evenly the space within which the movements are held (Wood and Marshall 1986; Challis and Kerwin 1992), using more than two cameras whenever possible and ensuring that the angle between the optical axis has enough width (Chen et al. 1994; Gourgoulis, Aggeloussis, Kasimatis, et al. 2008). Nevertheless, in many situations the image distortion cannot be neglected, such as in underwater analysis (Kwon 1999; Gourgoulis, Aggeloussis, Kasimatis et al. 2008; Silvatti, Cerveri, et al. 2012; Silvatti, Dias, et al. 2012).

Modifications to the original DLT were also proposed to account for lens distortion. Marzan and Karara (1975) increased the number of implicit parameters to 16 to account for the lens distortions, but their model used less terms to account distortion than recommended (Challis and Kerwin 1992). Hatze (1988) proposed two modified versions of the DLT (linear and nonlinear) that improved the accuracy of the DLT. However, given the higher order

*Corresponding author. Email: rossim03@student.uwa.edu.au

of nonlinearity, at least 30 CPs evenly distributed in the boundaries of the working volume were necessary (extrapolation resulted in poor results).

The Brown–Conrady model (Brown 1971; Clarke and Fryer 1998) states that in perspective projection, the image of a straight line will remain a straight line unless lens distortion is present, and, therefore, techniques mostly used to quantify lens distortion use deviations from straightness in the image. Several techniques were then developed following the straight-line model. A method proposed by Zhang (2000) uses a planar chequered pattern moved in front of the camera that enables calculation of the radial distortion parameters along with the intrinsic parameters of the camera. Bouguet (2004) developed a toolbox for Matlab based on Zhang's model that also yields the tangential parameters and also enables stereo calibration of two cameras, if the chequered pattern can be seen moving in front of both cameras simultaneously.

Once the distortion of the image can be corrected, it is expected that the accuracy of the DLT algorithm can be improved. It is not known, however, the extent to which the accuracy can be improved or whether by doing so the DLT becomes more flexible with regard to the number of CPs, extrapolation of the calibration volume or number/position of the cameras used. Therefore, the aim of this study was to analyse the accuracy of a robust method to determine and correct the lens distortion before using the DLT algorithm for camera calibration and 3D reconstruction. The accuracy was tested under different conditions of working volume (interpolation and extrapolation), camera focal length (4 and 8 mm) and number of CPs (8, 12, 18 and 162) used in the calibration procedure.

Methods

According to the Brown–Conrady model (Brown 1971; Clarke and Fryer 1998), lens distortion can be classified into radial distortion and tangential distortion. Radial distortion makes a point in the image to be displaced radially from or to the centre of the image; the greater is the distance from the centre of the image, the greater is the displacement from the expected position. Tangential distortion results from tilting between a set of lens (i.e. the centre of curvature of the lenses used is no collinear), which displaces the image coordinates in a direction normal to the radial lines emerging from the centre of the image. The principal point (i.e. the point in the image plane at the base of a line that passes through the focal point and is perpendicular to the image plane) can be assumed as the centre of the image for the pinhole camera model (Tsai 1987; Willson and Shafer 1994; Tapper et al. 2002). Brown (1971) proposed the mathematical model to determine lens distortion parameters through the images of straight lines. According to this model, the radial and tangential distortions can be calculated through the following equations:

$$\Delta x_i^{\mathrm{Rad}}(x_i, y_i) = x_i\left(k_1 r^2 + k_2 r^4 + k_3 r^6 + \cdots\right), \quad (1)$$

$$\Delta y_i^{\mathrm{Rad}}(x_i, y_i) = y_i\left(k_1 r^2 + k_2 r^4 + k_3 r^6 + \cdots\right), \quad (2)$$

$$\Delta x_i^{\mathrm{Tang}}(x_i, y_i) = p_1\left(3x_i^2 + y_i^2\right) + 2p_2 x_i y_i, \quad (3)$$

$$\Delta y_i^{\mathrm{Tang}}(x_i, y_i) = p_2\left(3y_i^2 + x_i^2\right) + 2p_1 x_i y_i, \quad (4)$$

where x_i and y_i are the error-free coordinates of the ith point in the plane of the image; $\Delta x_i^{\mathrm{Rad}}$, $\Delta y_i^{\mathrm{Rad}}$, $\Delta x_i^{\mathrm{Tang}}$ and $\Delta y_i^{\mathrm{Tang}}$ are the total displacement from the error-free coordinates of the ith point due to the radial and tangential distortions, respectively; $r = \sqrt{x_i^2 + y_i^2}$; $(k_1, k_2, k_3, \ldots, k_n)$ is an infinite series of parameters for the radial distortion (usually the equations do not have more than three parameters); and p_1 and p_2 are the two parameters for the tangential distortion.

Six plumb lines, each containing 27 retro-reflective CPs (10 cm apart from each other approximately; total of 162 CPs), were used to delimit a volume within which a one-cycle human gait can be analysed (2.7 m × 2.7 m × 0.9 m; 6.6 m^3) and to calculate the 11 implicit parameters of the DLT algorithm for each camera (Abdel-Aziz and Karara 1971). A rod containing two retro-reflective validation points (VPs, one for each extremity) was used in two dynamic trials (further explained). The distance between the pair of points (L_R), calculated by averaging 10 measures from centre to centre of the VPs obtained with a Vernier calliper (0.05 mm precision), was 285.024 ± 0.011 mm.

The DVIDEO™ kinematic analysis system (Figueroa et al. 2003; Miana et al. 2009; Sarro et al. 2009) was used to digitise the CPs during the static calibration trials, track automatically the VPs from the dynamic trials (further explained), calculate the DLT parameters for each camera and the 3D coordinates of the points of interest. The system used four synchronised digital cameras (Basler™ 602fc) connected to a workstation. As the dimensions of the charge-coupled device were 4.86 mm × 6.49 mm (490 × 656 pixels), and the cameras enabled manual adjustment for focal distances of 8 and 4 mm, the horizontal angle of view ($\alpha = 2\arctan(6.49/2f)$) used was approximately 45° and 78°, respectively.

For the distortion correction procedure, a chequered pattern containing 7 rows and 10 lines of squares (100 mm side) was moved in front of each camera to enable calculation of the distortion parameters (Figure 1). A Matlab™ toolbox developed by Bouguet (2004) was slightly modified to enable video analysis and automatic extraction of the square corners, which were used to determine the deviations from straightness of all the lines in the chequered pattern (available in http://calib.googl

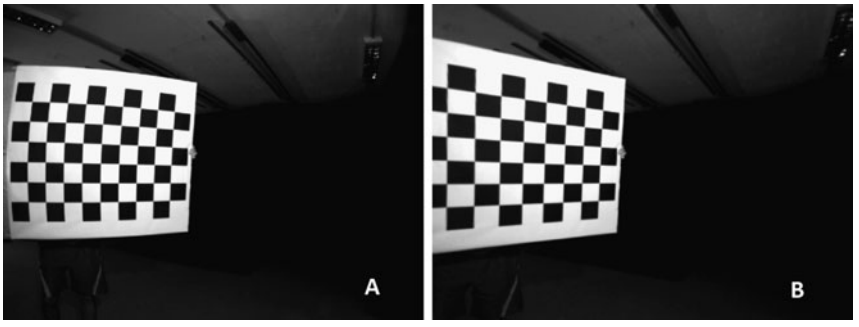

Figure 1. Images of the chequered pattern from camera 2 (Set-up 4) used to obtain the intrinsic and the distortion parameters, before (A) and after (B) the lens distortion correction procedure was applied.

ecode.com). At the end of this process, the toolbox enabled calculation of the radial (k_1, k_2 and k_3) and tangential (p_1 and p_2) distortion parameters along with the focal distance values and the coordinates of the principal point for each camera. The next step is the computation of the error-free point coordinates using the distortion parameters and the coordinates of the digitised points (CPs and VPs), referred as inverse mapping (Heikkila and Silven 1997).

Equations (1)–(4) enable calculation of the displacement from the error-free coordinates of a given point due to radical and tangential distortion, using the error-free coordinates as input. However, the aim is to find the error-free coordinates from the coordinates of the digitised points (back projection), and thus an approach such as the inverse mapping (Heikkila and Silven 1997) is required. Another toolbox was developed to calculate the corrected position of the markers, which used a normalisation function devised by Bouguet (2004) based on an iterative approach to carry out the inverse mapping (Heikkila and Silven 1997):

$$p_i = p_i' - \delta\left(p_i' - \delta(p_i')\right), \tag{5}$$

where p_i and p_i' are the coordinate vectors for the corrected and the distorted point position, respectively, and $\delta(p)$ is the function representing the distortion in image location p. Only after obtaining the corrected coordinates of the CPs or VPs, the DLT parameters and distance between the VPs can be calculated (Figure 2).

Four different camera set-ups were used to verify the influence of focal distance, number of cameras, camera position and extrapolation of the working volume (Figure 3). Set-up 1 used a pair of cameras (1 and 4) adjusted to an 8-mm focal distance (field of view of ~45°) and an angle of nearly 90° between the optical axes. Set-up 2 used another pair of cameras (2 and 3) adjusted to a 4-mm focal distance and a narrower angle (40°) between the optical axes. Set-up 3 used the cameras of Set-ups 1 and 2 simultaneously. Therefore, the same movement of the rod, which did not extrapolate the boundaries of the working volume, was used for the analysis of these three

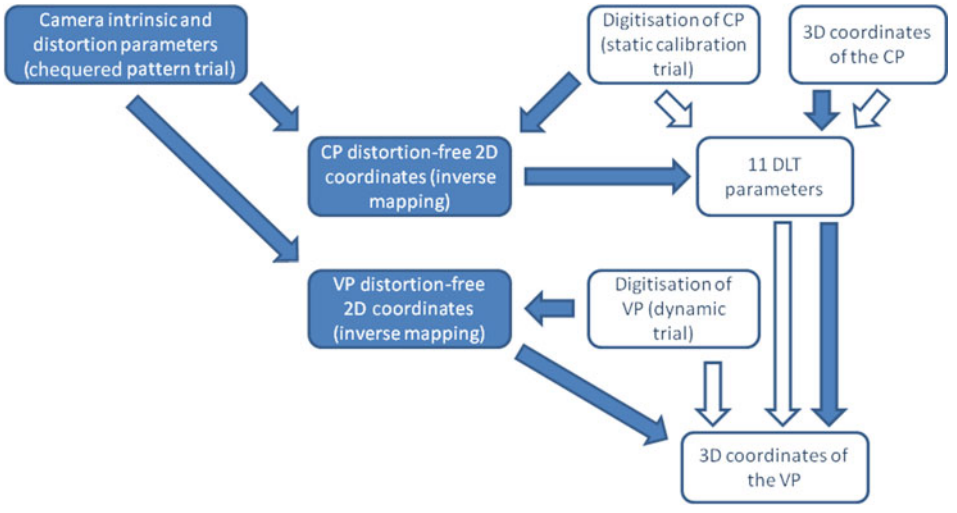

Figure 2. Flowchart explaining the two approaches for a single camera: the traditional DLT algorithm steps (following the blank arrows) and the DLT algorithm with previous correction for lens distortions (following the blue arrows).

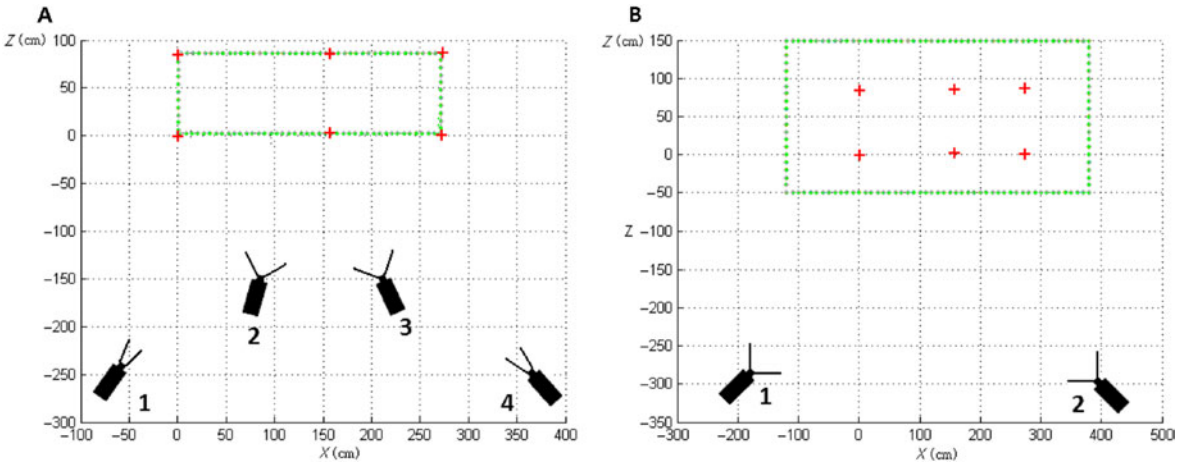

Figure 3. Position of the cameras relative to the working volumes in the transverse plane (*XZ*). On the left (A), position of the cameras for Set-ups 1 (cameras 1 and 4, 8 mm focal distance and wider angle between optical axes), 2 (cameras 2 and 3, 4 mm focal distance and narrower angle between optical axes) and 3 (using all four cameras). On the right (B), Set-up 4 (4 mm focal distance and wider angle between optical axes). Red crosses indicate the position of the plumb lines, whereas the green dots delimit the non-extrapolated calibration (volume 1, left), and the extrapolated volume (volume 2, right).

set-ups. For all the cameras, the field-of-view was such that all the CPs could be viewed. Set-up 4 aimed to verify the influence of the extrapolation of the working volume, and thus it used a pair of cameras adjusted to a 4-mm focal distance, positioned further away from the gait volume and angle between optical axes of about 90°. A total volume of 25 m^3 (5 m × 2 m × 2.5 m), within which the CPs were held, was used for the new rod movement.

For each camera set-up, the influence of the number of CPs was also assessed (Figure 4). Four different combinations of CPs were adopted: using all 162 CPs; 18 CPs, only using the highest, the lowest and the middle CPs of each plumb line; 12 CPs, using the highest and lowest CPs of each plumb line; and 8 CPs, only the CPs representing the corners of the gait volume.

Just for a better understanding of the lens distortion effects on the accuracy of the reconstructions, the rod's lengths were also calculated using the normal DLT algorithm (no correction procedure applied) and then compared with the results with distortion correction. Even though poorer accuracy is expected especially when some configurations are adopted (for instance, only eight CPs), the analysis helped identifying possible systematic effects of distortions and to which extent the correction procedure was able to minimise those effects.

The frame-by-frame reconstructions of the rod's length (L_i) obtained for every configuration were assessed by calculating the mean, median, standard deviation (SD) and variance (SD^2). The comparison of those values with the real length (L_R) was done by calculating the following errors: minimum (E_{Min}), maximum (E_{Max}), mean absolute (E_{Abs}, Equation (6)), root mean square (RMS, Equation (7)) and percent RMS $\left(\%RMS = RMS \times 100/L_R\right)$ errors. The first trial had $N = 262$ frames, whereas the second trial had $N = 1138$ frames.

$$E_{Abs} = \frac{\sum |L_R - L_i|}{N}, \tag{6}$$

$$E_{Abs} = \sqrt{\frac{\sum (L_R - L_i)^2}{N}}. \tag{7}$$

Results

The results are shown in Table 1. Overall, Set-up 1 performed better than Set-ups 2 and 3. It had pretty similar mean and SD values across CP configurations (Figure 5), as well as all %RMS values below 1% and E_{Abs} inferior to 2 mm. For this camera set-up, the quantity of CPs represents a minor issue for the accuracy of the measurements.

The accuracy of Set-up 2 was only satisfactory when all 162 CPs were used. With less CPs, %RMS and E_{Abs} of up to 3% and 7.5 mm, respectively, were found. These results seem to arise from a systematic increase of the mean length value and the SD (Figures 5 and 6) when less CPs were used. Therefore, when two 4-mm-focal-distance cameras were used with narrow angle between their optical axes, the lens distortion correction procedure will only yield accurate results when a fair number of CPs are used.

As a result of the latter, the accuracy of Set-up 3 (four cameras) was lower than that of Set-up 1, yet the results remained fairly accurate, with %RMS closer to 1% and

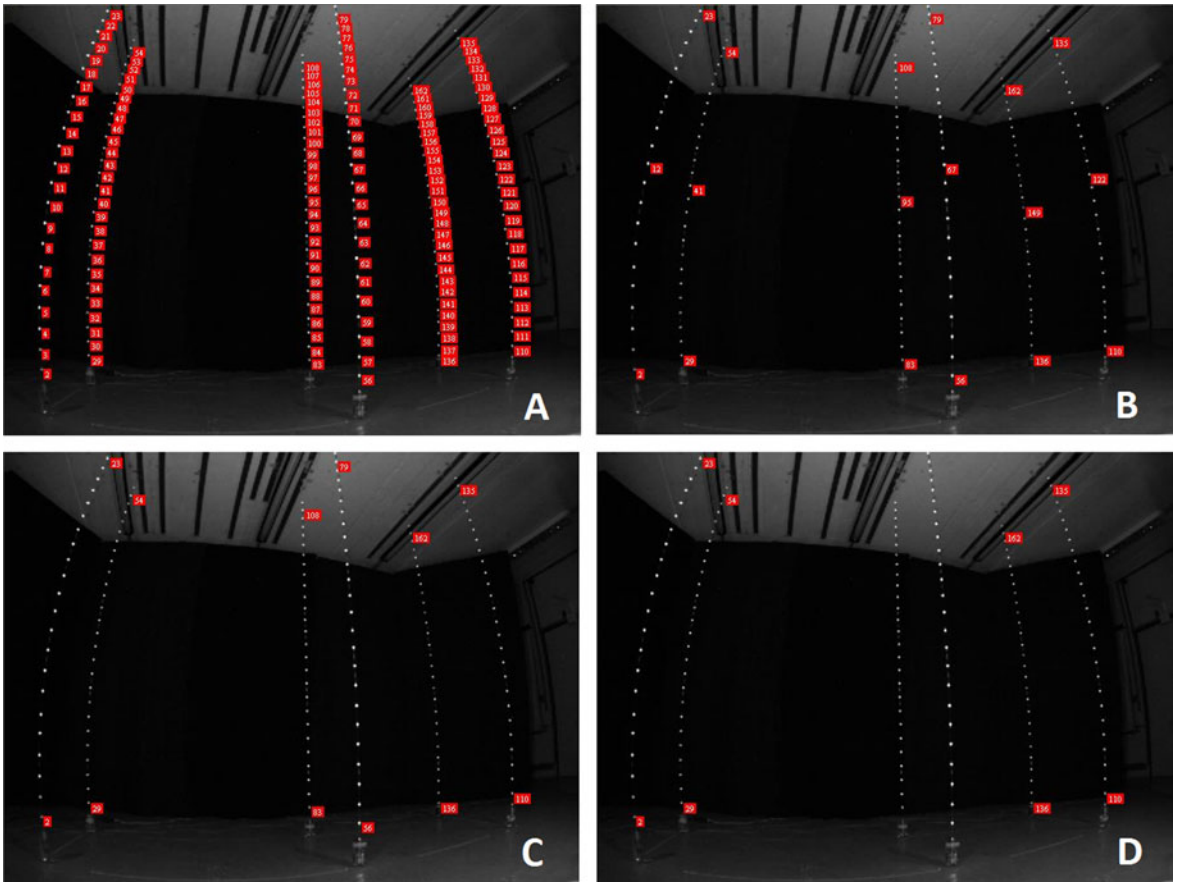

Figure 4. Image of the plumb lines from camera 2 (Set-ups 2 and 3) showing the amount of distortion when using the 4 mm focal distance and the four groups of calibration points: all CPs (A), 18 CPs (B), 12 CPs (C) and 8 CPs (D).

Table 1. Accuracy assessment of Set-up 1 (pair of cameras with 8 mm focal distance and wider angle between optical axes), Set-up 2 (pair of cameras with 4 mm focal distance and narrower angle between optical axes), Set-up 3 (both pairs of cameras used in Set-ups 1 and 2) and Set-up 4 (pair of cameras with 4 mm focal distance, wider angle between optical axes and extrapolation of the working volume), along with the quantity of CPs when reconstructing the rod's length after the lens distortion correction procedure (values presented in mm).

Camera set-up	No. of CPs	Mean	Median	SD	SD^2	E_{Min}	E_{Max}	E_{Abs}	RMS	RMS (%)
Set-up 1	All CPs	285.46	284.98	1.44	2.07	0.01	4.16	1.24	1.50	0.53
	18 CPs	284.19	283.64	1.47	2.17	0.00	5.05	1.33	1.69	0.59
	12 CPs	284.10	283.83	2.22	4.91	0.00	5.96	1.95	2.40	0.84
	8 CPs	284.11	283.80	2.22	4.93	0.04	5.95	1.95	2.40	0.84
Set-up 2	All CPs	285.65	285.26	1.98	3.94	0.00	9.51	1.57	2.08	0.73
	18 CPs	291.88	291.67	2.77	7.68	0.02	12.55	6.86	7.40	2.60
	12 CPs	292.48	292.56	4.90	23.99	0.05	19.52	7.52	8.91	3.13
	8 CPs	292.41	292.18	2.87	8.23	0.19	12.91	7.39	7.92	2.78
Set-up 3	All CPs	285.13	284.97	1.92	3.69	0.01	5.15	1.54	1.92	0.67
	18 CPs	288.06	287.41	1.55	2.40	0.02	7.26	3.04	3.41	1.20
	12 CPs	286.65	286.46	1.49	2.22	0.05	5.04	1.78	2.21	0.77
	8 CPs	287.74	287.05	1.50	2.24	0.03	6.80	2.73	3.10	1.09
Set-up 4	All CPs	286.65	286.51	3.80	14.45	0.14	15.15	3.25	4.13	1.45
	18 CPs	284.95	284.90	4.04	16.34	0.12	13.97	3.25	4.04	1.42
	12 CPs	285.23	285.21	4.21	17.75	0.06	13.30	3.39	4.22	1.48
	8 CPs	285.60	285.65	4.83	23.31	0.16	16.17	3.91	4.86	1.71

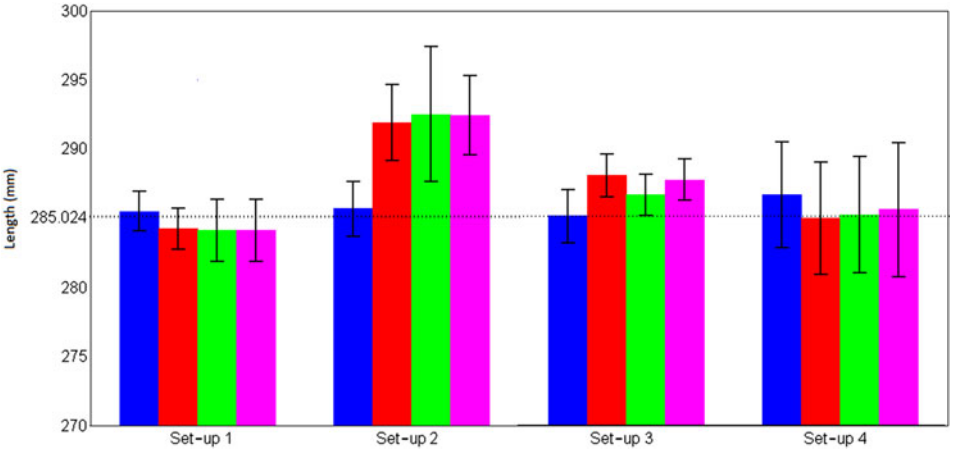

Figure 5. Mean and SD (in mm) of the rod's length reconstructions for Set-up 1 (8 mm focal distance/wider angle between optical axes), Set-up 2 (4 mm focal distance/narrower angle between optical axes), Set-up 3 (Set-ups 1 and 2 together) and Set-up 4 (4 mm focal distance/wider angle between optical axes/extrapolation of the working volume) along with the number of CPs used. Real rod's length = 285.024 mm.

E_{Abs} of up to 3 mm. The slight rise of the mean and SD length values when less CPs are used might have been a result of the DLT algorithm trying to compensate for the errors of Set-up 2 pair. Still, the results indicate a fairly accurate camera set-up, and the number of CPs used does not seem to jeopardise the accuracy of the measures.

When the working volume was extrapolated (Set-up 4), the results showed close mean, median and SD values for the three CP groups, and %RMS and E_{Abs} of about 1.50% and 3 mm, respectively. The eight-CP configuration performed slightly worse than the other groups for this set-up, yet the distortion correction procedure enabled results that were noteworthy better than it would be expected without correction. Moreover, it is important to verify that overall this camera configuration had better accuracy than Set-up 2, indicating that the lens distortion

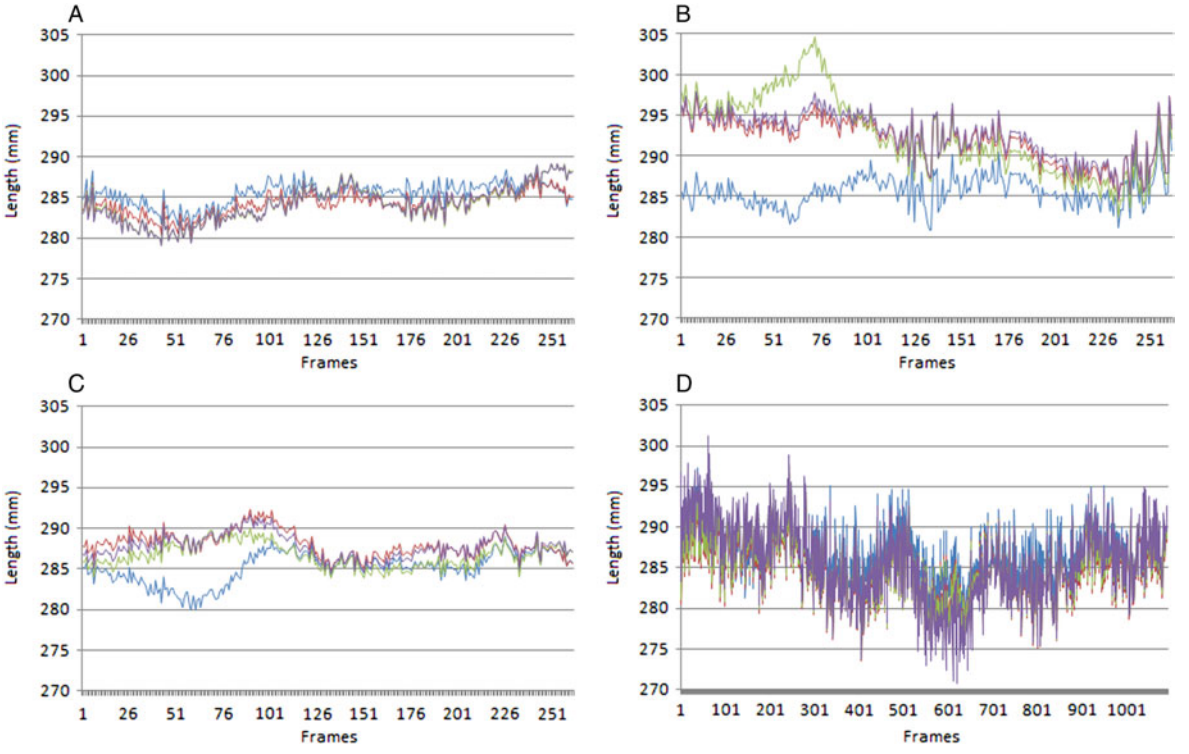

Figure 6. The rod's length (in mm) reconstruction in function of time for Set-up 1 (A), Set-up 2 (B), Set-up 3 (C) and Set-up 4 (D). For each graph, the lines represented the reconstructions using all CPs (blue), 18 CPs (red), 12 CPs (green) and 8 CPs (purple).

correction procedure had good effectiveness when using this type of wide-angle lenses.

The effectiveness of the lens distortion correction procedure can be easily noticed when compared with the rod reconstructions without it (Figure 7). The systematic effects of lens distortion, which resulted in the humpy pattern of the curves, almost completely disappeared once the correction procedure was applied. The pattern of the curves without correction is the same for Set-ups 1, 2 and 3.

Discussion

The aims of the study were to access a distortion correction procedure to the digitised points before calculation of the DLT parameters and 3D coordinates of the analysed points, and to verify whether the procedure improves the accuracy of the DLT method. The greater advantage of this procedure is that it involves just a chequered planar pattern that can be easily designed and built and two toolboxes for Matlab™. If by correcting the distortion effects the movement analysis can also be conducted outside the boundaries of the calibration volume and less CPs are needed, smaller and simpler calibration structures can be constructed, minimising concerns with transport and storage, and thereby yielding more robust results with greater flexibility and lower costs (Zhang 2000).

The %RMS values found for Set-ups 1, 3 and 4 when the distortion correction procedure is applied are compatible with other values found for the normal DLT algorithm in the literature (Yanai et al. 1996; Gourgoulis, Aggeloussis, Kasimatis, et al. 2008). However, one important characteristic to point out about the previous studies is the focal lengths used. Even though the values were not informed, it can be assumed from the characteristics of the set-ups that those were cameras with telephoto lenses, which means greater focal distance and narrower field of view. Therefore, in order to fit the whole calibration frame within the image, the camera has to be placed further away from it. In the study of Gourgoulis, Aggeloussis, Kasimatis, et al. (2008), the camera had to be positioned 12 m away from a 3-m-long calibration. It might be disadvantageous in situations when the specificity of the analysed movement or the constraints of the environment demand closer distance between camera and the movement (for instance, a camera placed at the bottom of a pool to record a swimmers' movement on the frontal plane). The reason why telephoto lenses are a better option than wide-angle lenses when using the DLT is because there is a very close to linear relationship between angles inferior to 10° and their respective sines. According to Snell–Descartes Law, the rate of the sines of the angles of incidence and refraction is equivalent to the opposite ratio of the indices of refraction. Therefore, the relationship between the angle of incidence and the angle of refraction (both relative to the optical axis of the camera) is linear when the field of view is narrower than 20°, which enables the DLT algorithm to compensate for refraction.

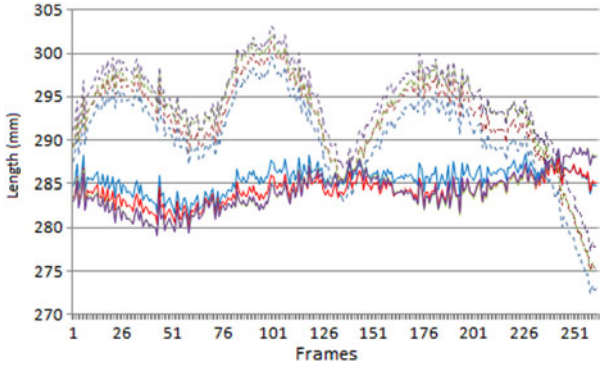

Figure 7. Results obtained with Set-up 1 when lens distortion correction is not applied (dashed lines) and when it was applied (continuous lines). The lines represent the configurations of CPs when using all CPs (blue), 18 CPs (red), 12 CPs (green) and 8 CPs (purple).

This linear relationship disappears when the field of view is greater than 20°, which results in greater distortion closer to the image border. The cameras used in this study had fields of view of 45° and 78°, for the 8 and 4-mm focal length pairs, respectively. As a result of that, the CPs positioned closer to the borders (as the aim is to magnify the dimensions of the calibration frame in the image) had their coordinates affected by distortion. Figure 7 shows exactly what happened to the reconstructions of Set-up 1 when the lens distortion correction factor was not applied (the curve patterns are exactly the same for Set-ups 2 and 3). Local maxima were attained whenever the rod passed in the horizontal middle of the image, whereas local minima were attained whenever the rod got as close as possible to the borders. That results from radial distortion, as the greater is the distance from the centre of the image, the greater is the displacement (distortion) towards the centre of the image, which shrinks the objects closer to the border.

Another source of systematic error was the displacement of the curves towards the top of the graph as the number of CPs decreases. The eight-CP configuration only had CPs in the corners of the calibration volume, and as they were too close to the border, they suffered great amount of distortion. These distorted coordinates made the DLT algorithm to interpret the image of the calibration volume as smaller than it actually was. As a result of that, the rod's length was overestimated. A large number of CPs (closer to the midline of the image) helped the DLT algorithm to find a more realistic best-fit solution for the dimensions of the calibration volume, therefore, the rod's reconstruction curves were shifted downwards.

The lens distortion correction procedure minimised substantially the rod's reconstruction error, as it can be

seen in Figures 6 and 7. Set-ups 1, 3 and 4 had flatter reconstruction lines of the graphs (relatively small humps can be perceived, indicating that there is still some residual effect of systematic distortion), and also the vertical distances between these lines almost completely disappeared. Despite the more enhanced curves in Set-up 4, it seems that random errors contributed more to the inferior performance compared with Set-ups 1 and 3, as the mean values were all close to the real rod length for all CP groups, but the variance was markedly greater. As both images of the rod and the plumb lines were smaller in this configuration, it was more susceptible to errors during the digitisation. Moreover, when an extra pair of cameras with very similar intrinsic and extrinsic parameters (i.e. same focal distance, position and orientation of the first pair, as they were placed right below the pair used in Set-up 4) was used to reconstruct the same rod's movement, the %RMS and E_{Abs} improved to just 1% and less 2.5 mm, respectively, for all CPs, 18 CPs and 12 CPs, and even the 8-CP configuration with the four cameras had better accuracy than using all CPs with just two cameras. Therefore, yet the distortion correction procedure cannot eliminate completely the systematic effects of lens distortions, wide-angle-camera set-ups can yield accurate results when more cameras (or even cameras with greater resolution) are used and placed in the right position relative to each other. These findings are very promising with regard to a more flexible video-based 3D analysis of movements, as the correction procedure now enables the design and construction of considerably smaller calibration frames containing less CPs, and cameras with great field of view can be used. Moreover, no further modification has to be carried out in image-based systems that use the traditional DLT algorithm, it only needs a Matlab™ toolbox that can be downloaded freely (available in http://calib.googlecode.com), and the chequered pattern can be easily designed and built (i.e. one only needs to print the pattern in a sheet of paper and stick it to a planar surface).

The procedure did not work so well for Set-up 2, even though it gave a more linear pattern for the curve in the graph (Figure 6). Two distinct characteristics between Set-up 2 and the others are (i) increased noise in the reconstruction curve and (ii) noteworthy (yet smaller than if no correction is applied) vertical displacement of the curve with different number of CPs. Noise arises from random errors, and possible explanation for it would be the narrow angle between the optical axes of the cameras. The resolution of a given distance in the image may be different in one Cartesian direction than in the other two, and, therefore, random errors during digitisation caused larger errors in the direction with lower resolution (Gourgoulis, Aggeloussis, Kasimatis, et al. 2008). The explanation for the systematic vertical shift of the curves might be twofold. First, no lens distortion correction procedure is capable of completely eradicating the distortions, which may in part explain the larger number of humps for all the CP configurations in the second trial, and the best performance possible may have not been enough to correct the coordinates of the plumb line's and the rod's points when they were close to the borders in a 4-mm focal distance camera. Thus, even after the correction procedure, the CPs might have been closer to the centre of the image than they should, which reduced its real dimensions in the image, an effect minimised when more points were used, as previously explained. Second, the random errors during digitisation of the distorted CPs might have been magnified after the distortion correction procedure, and thus only eight points were not enough to minimise this magnification, and the dimensions of the calibration space were wrongly interpreted by the DLT algorithm. When more CPs were used, specifically those at the regions of the image less affected by distortion, the rod's reconstruction curves were brought to a closer and more optimal vertical position. Another possible approach to minimise this problem, although more computationally expensive, would be first correcting the image distortion and then digitising the points, rather than doing the opposite way (i.e. conducting the digitisation in the distorted image and then just correcting the digitised points). As in Set-up 4, the CPs were not so close to the borders, they were less affected by distortion and also the correction procedure may have produced less magnification of the digitising random errors, which may explain its better performance.

A synthesis of the findings is presented in Table 2.

This method is similar to the method proposed by Tsai (1987), as it is based on the pinhole camera model, and the last two of the four coordinate transformations are referred during the inverse mapping. However, Tsai (1987) used the calibration pattern (planar structure with several black squares whose corners are used as calibration points) as a fixed global coordinate system and then the algorithm creates an over-determined system with a linear equation for each calibration point based on the radial alignment constraint and thus providing the internal and external camera parameters. Our method used a moving chequerboard pattern placed at various orientations to compute the internal parameters individually to each camera, minimising errors arising from improper visualisation of the square corners, and then the external parameters are computed using the DLT algorithm and the distortion-free coordinates of a fixed calibration object. Also, the Tsai method (Tsai 1987) only used the second-order term for radial distortion, whereas the present model used up to the sixth-order term and two further tangential distortion components.

Other calibration methods for large volumes and different focal distances are the wand-based methods used in many 3D commercial systems (Vicon, Oxford, UK; BTS, Milan, Italy) and consist of moving a rigid bar

Table 2. Synthesis of the findings when assessing different operational conditions.

Set-up	Characteristics	Influence of number of CPs over accuracy	Conclusion
Set-up 1	• Two cameras • Wide angle between optical axes (90°) • Wide field of view angle (45°) • Interpolated working volume	Great accuracy regardless the number of CPs (just a slight increase from few to many CPs)	This set-up minimises both systematic (lens distortion) and random (camera position and image resolution of the measured object) sources of errors. Few CPs are just enough.
Set-up 2	• Two cameras • Narrow angle between optical axes (40°) • Very wide field of view angle (78°) • Interpolated working volume	Many CPs are necessary for a good accuracy	This set-up minimises the systematic errors, but residual distortion still influences overall accuracy. Great influence of random errors due to narrow angle between optical axes. Many CPs are needed for great accuracy.
Set-up 3	• Four cameras • Combination of both pair of cameras used in Set-ups 1 and 2 • Interpolated working volume	Good accuracy regardless the number of CPs (just a slight increase from few to many CPs)	Combination of both Set-ups 1 and 2 does not yield the greatest accuracy, but it still provides good accuracy and the number of CPs is not influential.
Set-up 4	• Two cameras • Wide angle between optical axes (90°) • Very wide field of view angle (78°) • Extrapolated working volume	Lower accuracy regardless the number of CPs (just a slight increase from few to many CPs)	This set-up minimises the systematic errors, but residual distortion still influences overall accuracy. Random errors mainly result from the small images of the calibration object and the rod. The accuracy cannot be substantially increased with many CPs, but it is likely to increase with a larger number of cameras.

(wand) with markers to be tracked within the working volume. When the wand carries two markers, the distance between both is known, enabling the algorithm to compute the external parameters and the focal length of the cameras from the epipolar constraint (Cerveri et al. 1998), whereas when the bar has only one marker, a known rigid structure (smaller than that used in this method) containing CPs is used along with the DLT algorithm as initial guess for the camera parameters, which are refined using the bundle adjustment approach when the data from the dynamic trial of the wand are inputted to the algorithm (Silvatti, Dias, et al. 2012). The greatest advantage of these methods is the higher portability; on the other hand, the wand must be moved ensuring the whole calibration volume is covered and the accuracy is dependent on the construction of the calibration objects used (Silvatti, Dias, et al. 2012).

This method has a great potential to be applied specially in environments where modern passive optical analysis systems cannot be used, such as underwater analysis (Silvatti, Cerveri, et al. 2012; Silvatti, Dias, et al. 2012). The distortion that arises from the methods to capture underwater movements (e.g. house holding, pool windows and periscopes) has been explored in several studies (Kwon 1999; Lavest et al. 2003; Gourgoulis, Aggeloussis, Kasimatis, et al. 2008; Silvatti et al. 2010). Lavest et al. (2003) proved that it is possible to calibrate out-of-the-water-cameras to be submerged, as the focal distance and the magnitude of the distortions out of the water are amplified by a factor numerically equal to the index of refraction of water. Silvatti and colleagues (Silvatti et al. 2010; Silvatti, Cerveri, et al. 2012; Silvatti, Dias, et al. 2012) applied the present methodology in 3D analysis and found %RMS inferior to 1%, all comparable with the results obtained with a moving wand with nonlinear camera model and bundle adjustments, which ascertains its applicability for analyses of activities such as swimming. Even though the chequered pattern and the rod used to calibrate the system may be regarded as cumbersome compared with the wand method, the method enables calibration of both water and aerial environments, enabling full 3D analysis of a swimming movement.

Conclusion

The lens distortion correction applied to all CPs and VPs previous to the calculation of the DLT implicit parameters and the 3D reconstruction of the movement reduced the systematic errors substantially. Also, it made the apparatus needed for accurate 3D analysis less cumbersome, as few CPs and smaller calibration frames are less likely to jeopardise the accuracy. Cameras with larger fields of view can also be brought closer to the analysis volume; however, caution must be taken when using cameras with extreme fields of view, and it remains important to keep optimal angles between the optical axes to avoid inaccuracies due to random errors.

Notes

1. Email: amandasilvatti@yahoo.com.br
2. Email: diasf@esiee.fr
3. Email: ricardo@fef.unicamp.br

References

Abdel-Aziz YI, Karara HM. 1971. Direct linear transformation from comparator coordinates into object space coordinates in close range photogrammetry. In: Paper presented at: ASP1971. Proceedings of the Symposium on Close Range Photogrammetry. Falls Church (VA): American Society of Photogrammetry. p. 1–18.

Allard P, Stokes I, Blanchi J. 1995. Three-dimensional analysis of human motion. Champaign (IL): Human Kinetics.

Arellano R, Brown P, Cappaert J, Nelson R. 1994. Analysis of 50-, 100-, and 200-m freestyle swimmers at the 1992 Olympic Games. J Appl Biomech. 10(2):189–199.

Bouguet JY. 2004. Camera calibration toolbox for Matlab™ [Internet]. Pasadena (CA): Computer Vision Research Group, Department of Electrical Engineering California Institute of Technology; [cited 2009 Mar 15]. Available from: http://www.vision.caltech.edu/bouguetj/calib_doc/

Brown D. 1971. Close-range camera calibration. Phot Eng. 37 (8):855–866.

Cerveri P, Borghese N, Pedotti A. 1998. Complete calibration of a stereo photogrammetric system through control points of unknown coordinates. J Biomech. 31(10):935–940.

Challis JH, Kerwin DG. 1992. Accuracy assessment and control point configuration when using the DLT for photogrammetry. J Biomech. 25(9):1053–1058.

Chen L, Armstrong CW, Raftopoulos DD. 1994. An investigation on the accuracy of three-dimensional space reconstruction using the direct linear transformation technique. J Biomech. 27(4):493–500.

Clarke T, Fryer J. 1998. The development of camera calibration methods and models. Photgramm Rec. 16(91):51–66.

Coleman SGS, Rankin AJ. 2005. A three-dimensional examination of the planar nature of the golf swing. J Sports Sci. 23 (3):227–234.

Elliott B, Alderson J. 2007. Laboratory versus field testing in cricket bowling: a review of current and past practice in modelling techniques. Sports Biomech. 6(1):99–108.

Elliott B, Fleisig G, Nicholls R, Escamilia R. 2003. Technique effects on upper limb loading in the tennis serve. J Sci Med Sport. 6(1):76–87.

Figueroa PJ, Leite NJ, Barros RML. 2003. A flexible software for tracking of markers used in human motion analysis. Comput Metods Programs Biomed. 72(2):155–165.

Fleisig G, Nicholls R, Elliott B, Escamilla R. 2003. Kinematics used by world class tennis players to produce high-velocity serves. Sports Biomech. 2(1):51–64.

Gourgoulis V, Aggeloussis N, Kasimatis P, Vezos N, Boli A, Mavromatis G. 2008. Reconstruction accuracy in underwater three-dimensional kinematic analysis. J Sci Med Sport. 11 (2):90–95.

Gourgoulis V, Aggeloussis N, Vezos N, Kasimatis P, Antoniou P, Mavromatis G. 2008. Estimation of hand forces and propelling efficiency during front crawl swimming with hand paddles. J Biomech. 41(1):208–215.

Hatze H. 1988. High-precision three-dimensional photogrammetric calibration and object space reconstruction using a modified DLT-approach. J Biomech. 21(7):533–538.

Heikkila J, Silven O. 1997. A four-step camera calibration procedure with implicit image correction. Paper presented at: IEEE 1997.Proceedings of the Computer Society Conference on Computer Vision and Pattern Recognition; San Juan, Puerto Rico.

Kwon YH. 1999. Object plane deformation due to refraction in two-dimensional underwater motion analysis. J Applied Biomech. 15(4):396–403.

Kwon YH, Casebolt JB. 2006. Effects of light refraction on the accuracy of camera calibration and reconstruction in underwater motion analysis. Sports Biomech. 5(2):315–340.

Lauder M, Dabnichki P, Bartlett R. 2001. Improved accuracy and reliability of sweepback angle, pitch angle and hand velocity calculations in swimming. J Biomech. 34(1):31–39.

Lavest JM, Rives G, Lapresté JT. 2003. Dry camera calibration for underwater applications. Mach Vision Appl. 13 (5):245–253.

Marzan G, Karara H. 1975. A computer program for direct linear transformation solution of the colinearity condition, and some applications of it. Proceedings of the Symposium on Close Range Photogrammetric Systems; Falls Church, VA, USA.

Miana A, Prudêncio M, Barros R. 2009. Comparison of protocols for walking and running kinematics based on skin surface markers and rigid clusters of markers. Int J Sports Med. 30 (11):827–833.

Sanders R, Cappaert J, Devlin R. 1995. Wave characteristics of butterfly swimming. J Biomech. 28(1):9–16.

Sarro KJ, Silvatti AP, Aliverti A, Barros RML. 2009. Proposition and evaluation of a novel method based on videogrammetry to measure three-dimensional rib motion during breathing. J Appl Biomech. 25(3):247–252.

Silvatti AP, Cerveri P, Telles T, Dias FAS, Baroni G, Barros RML. 2012. Quantitative underwater 3D motion analysis using submerged video cameras: accuracy analysis and trajectory reconstruction. Comput Metods Biomech Biomed Eng. 16(11):1–9.

Silvatti AP, Dias FAS, Cerveri P, Barros RML. 2012. Comparison of different camera calibration approaches for underwater applications. J Biomech. 45(6):1112–1116.

Silvatti AP, Telles T, Rossi MM, Dias FAS, Leite NJ, Barros RML. 2010. Underwater non-linear camera calibration: an accuracy analysis. Paper presented at: ISBS 2010. Proceedings of the XXVIII International Symposium on Biomechanics in Sports; Marquette, MI, USA.

Tapper M, McKerrow PJ, Abrantes J. 2002. Problems encountered in the implementation of Tsai's algorithm for camera calibration. Proceedings of the 2002 Australasian Conference on Robotics and Automation; Auckland, New Zealand.

Tsai RA. 1987. A versatile camera calibration technique for high-accuracy 3D machine vision metrology using off-the-shelf TV cameras and lenses. IEEE J Robot Automat. 3(4):323–344.

Willson RG, Shafer SA. 1994. What is the center of the image? J Opt Soc Am A. 11(11):2946–2955.

Wood GA, Marshall RN. 1986. The accuracy of DLT extrapolation in three-dimensional film analysis. J Biomech. 19(9):781–785.

Yanai T, Hay J, Gerot J. 1996. Three-dimensional videography of swimming with panning periscopes. J Biomech. 29 (5):673–678.

Zhang Z. 2000. A flexible new technique for camera calibration. IEEE Trans Pattern Anal Mach Intell. 22(11):5–26.